Supporting Information

Unprecedented Ag-Cu_2O composited mesocrystals with efficient charge separation and transfer as well as visible light harvesting for enhanced photocatalytic activity

Shaodong Sun*, Xiaochuan Zhang, Xiaojing Yu, Jie Cui, Man Yang, Qing Yang, Peng Xiao and Shuhua Liang*

Engineering Research Center of Conducting Materials and Composite Technology, Ministry of Education; Shaanxi Engineering Research Centers of Metal-Based Heterogeneous Materials and Advanced Manufacturing Technology; Shaanxi Province Key Laboratory for Electrical Materials and Infiltration Technology; School of Materials Science and Engineering, Xi'an University of Technology, Xi'an 710048, Shaanxi, People's Republic of China.

Email: sdsun@xaut.edu.cn (S. D. Sun); liangsh@xaut.edu.cn (S. H. Liang).

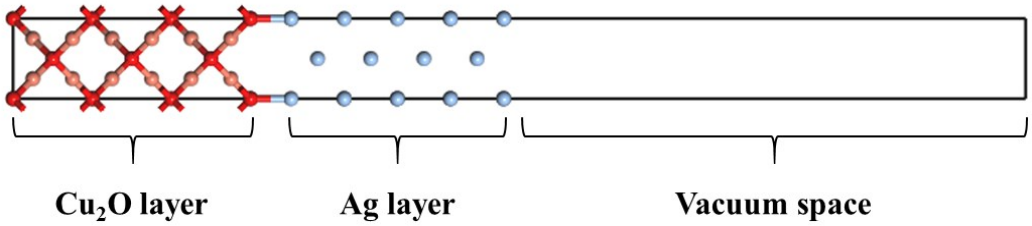

Figure S1. Periodic slab model of the Cu_2O-Ag interface

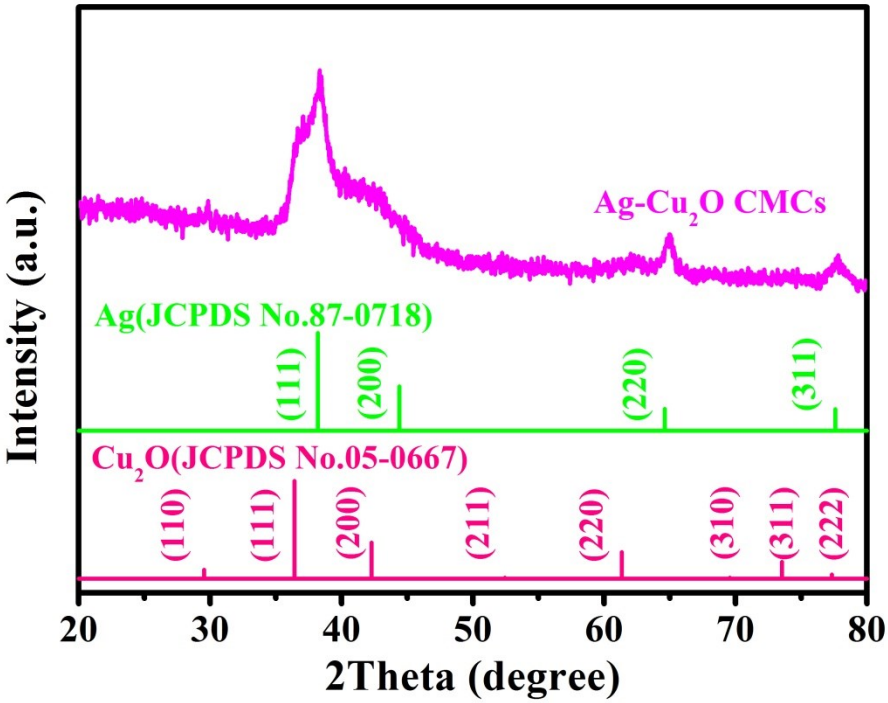

Figure S2. XRD pattern of the as-synthesized plate-like Ag-Cu_2O nanocomposite mesocrystals.

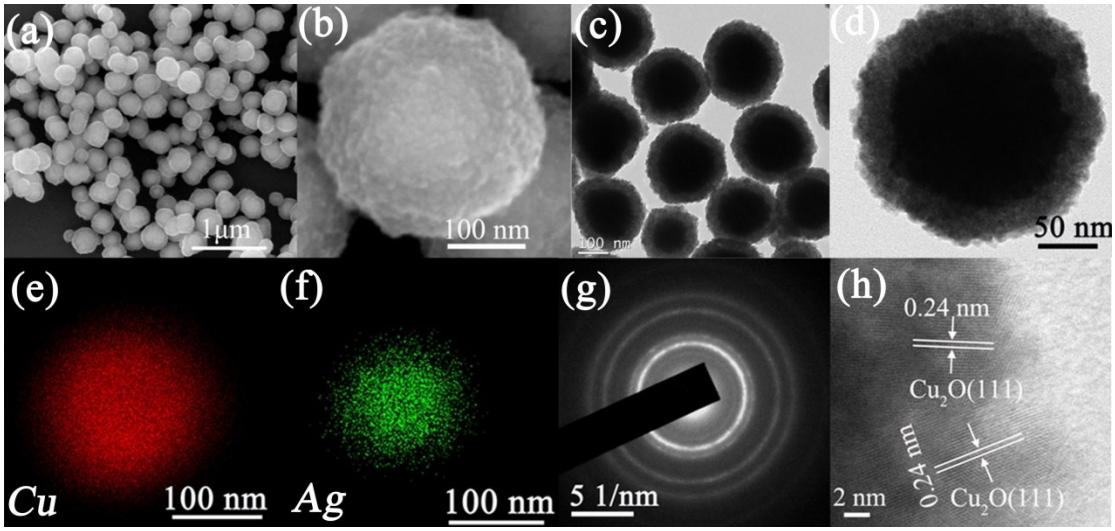

Figure S3. Microstructure characterizations of Ag@Cu_2O nanospheres. (a) Low-magnification SEM image; (b) High-magnification SEM image; (c) Low-magnification TEM image; (d) High-magnification SEM image; (e) and (f) Element mapping results of Cu and Ag species, respectively; (g) SAED pattern obtained from the nanosphere as shown in Figure S3d; (h) HRTEM image obtained from the edge of the nanosphere as shown in Figure S3d.

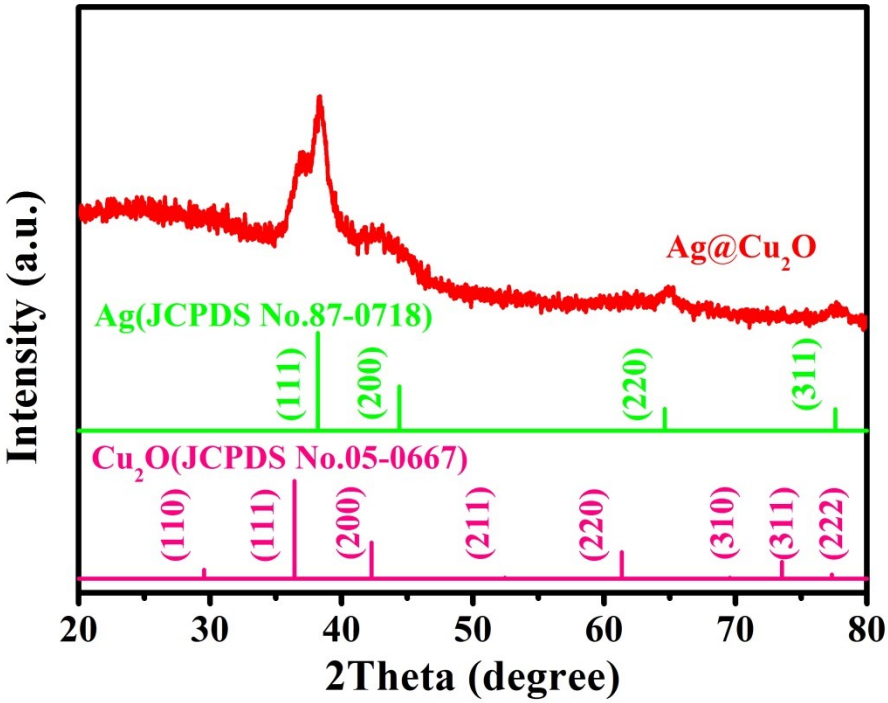

Figure S4. XRD pattern of the core-shell Ag@Cu_2O nanospheres as shown in Figure S3.

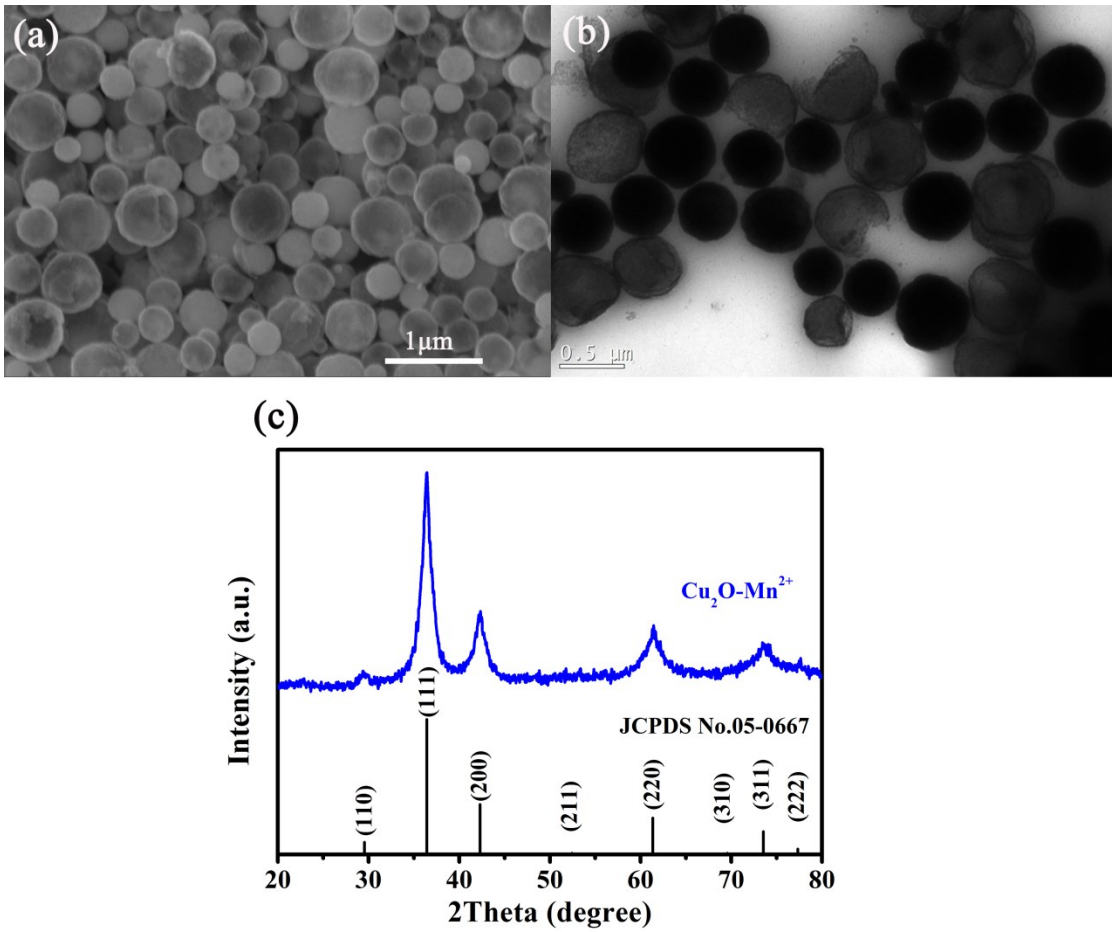

Figure S5. Microstructure characterizations of products obtained in the absence of Ag^+ ions. (a) Low-magnification SEM image; (b) low-magnification TEM image; (c) The corresponding XRD pattern.

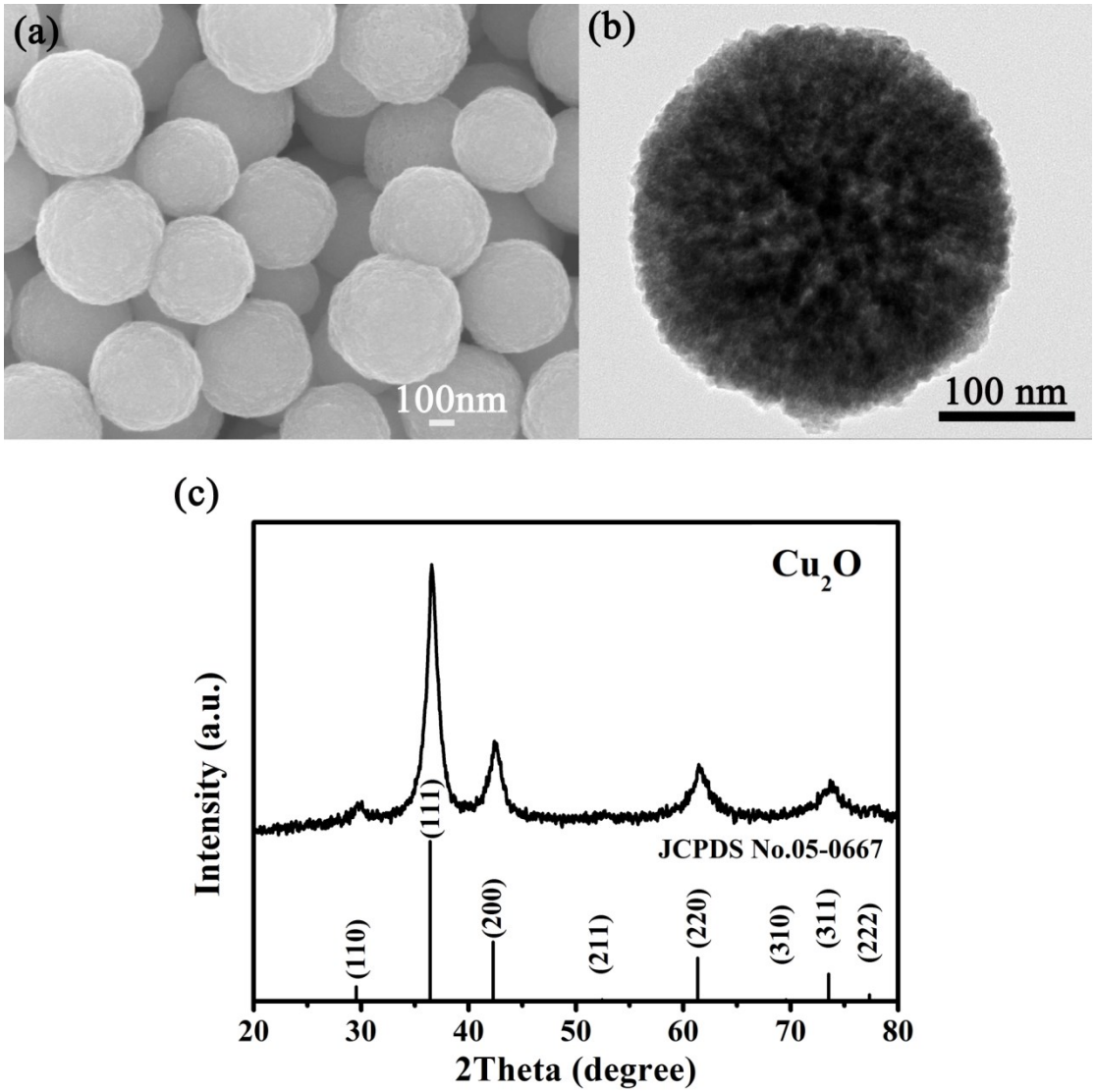

Figure S6. Microstructure characterizations of products obtained in the absence of Ag^{+} and Mn^{2+} ions. (a) Low-magnification SEM image; (b) low-magnification TEM image; (c) The corresponding XRD pattern.

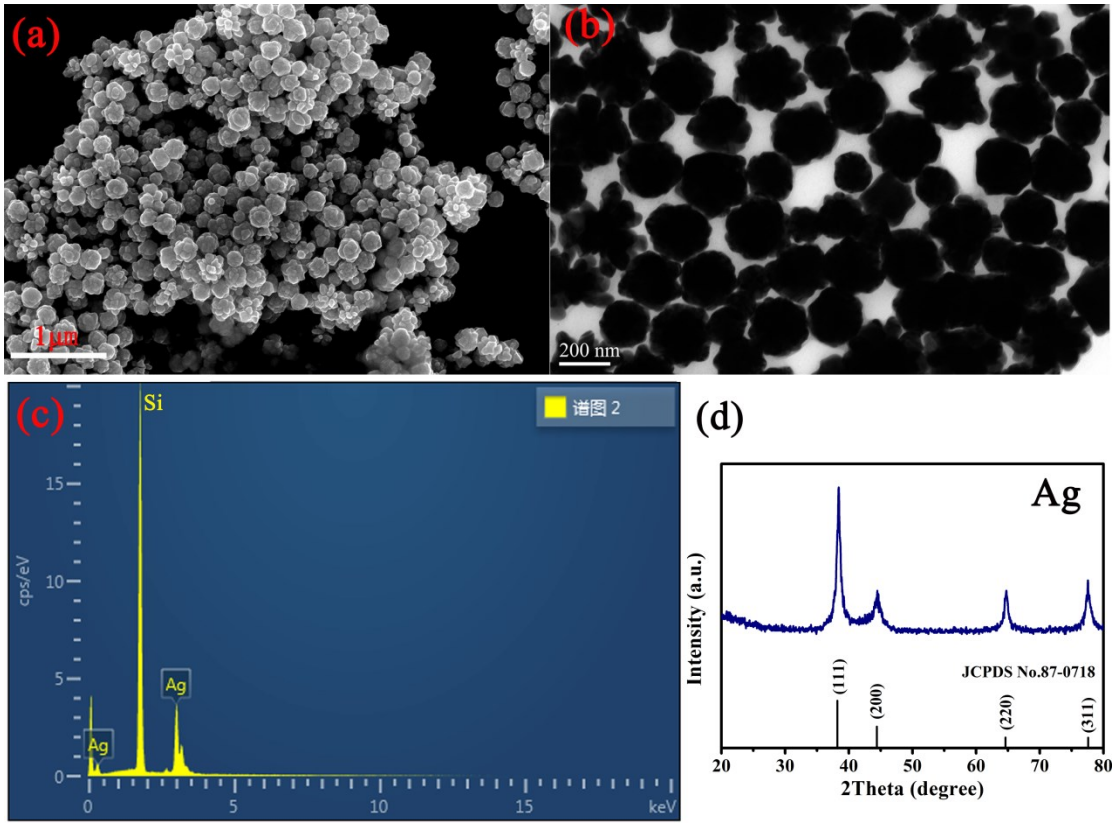

Figure S7. Microstructure characterizations of products obtained in the absence of Cu^{+} and Mn^{2+} ions. (a) Low-magnification SEM image; (b) low-magnification TEM image; (c) The corresponding EDS pattern; (d) The corresponding XRD pattern.

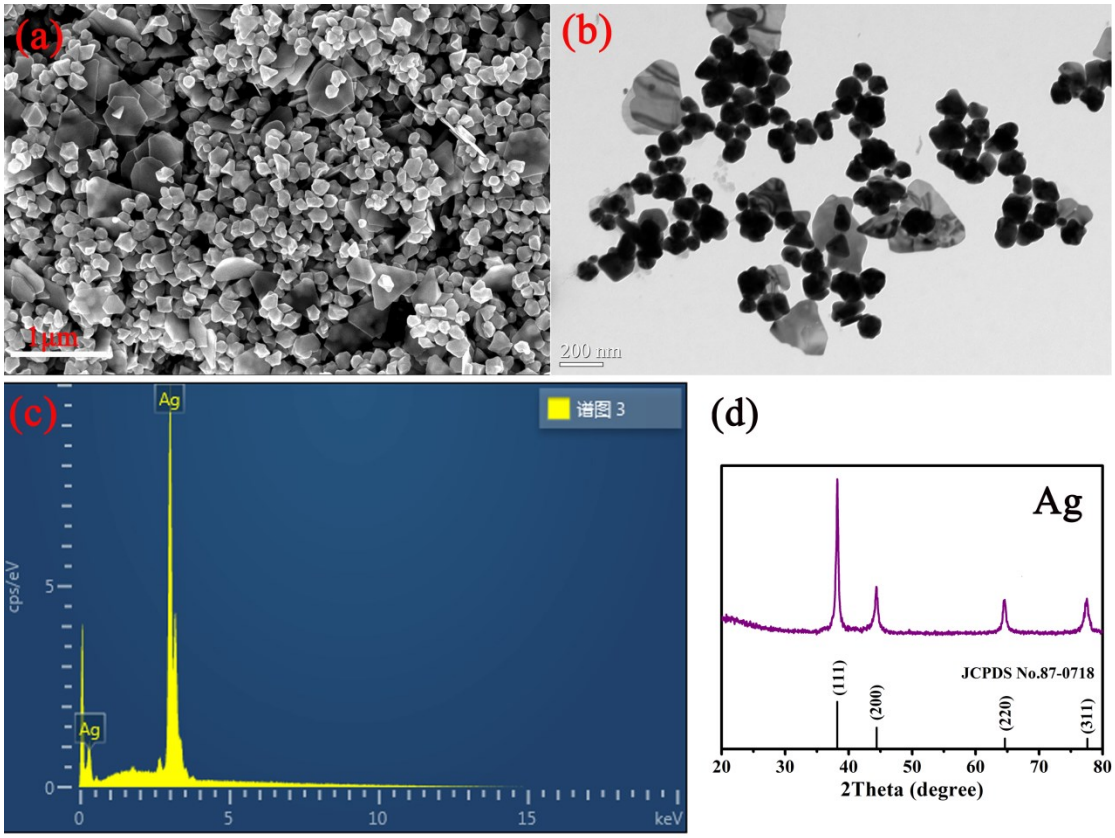

Figure S8. Microstructure characterizations of products obtained in the absence of Cu^{+} ions. (a) Low-magnification SEM image; (b) low-magnification TEM image; (c) The corresponding EDS pattern; (d) The corresponding XRD pattern.

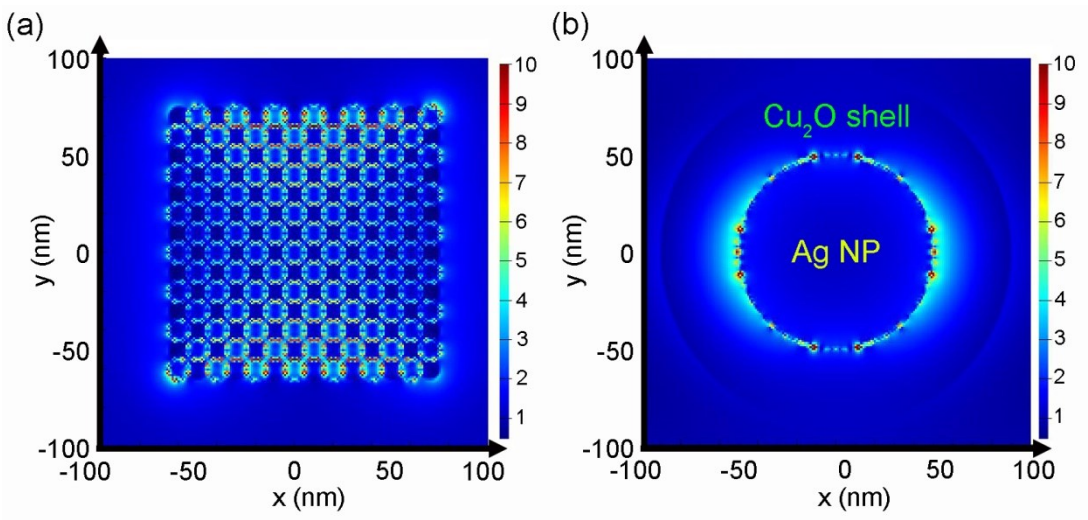

Figure S9. The 3D-FDTD simulated electric-field spatial distribution on the x–y plane for (a) Ag-Cu_2O CMCs, (b) Ag@Cu_2O core-shell structure, respectively.

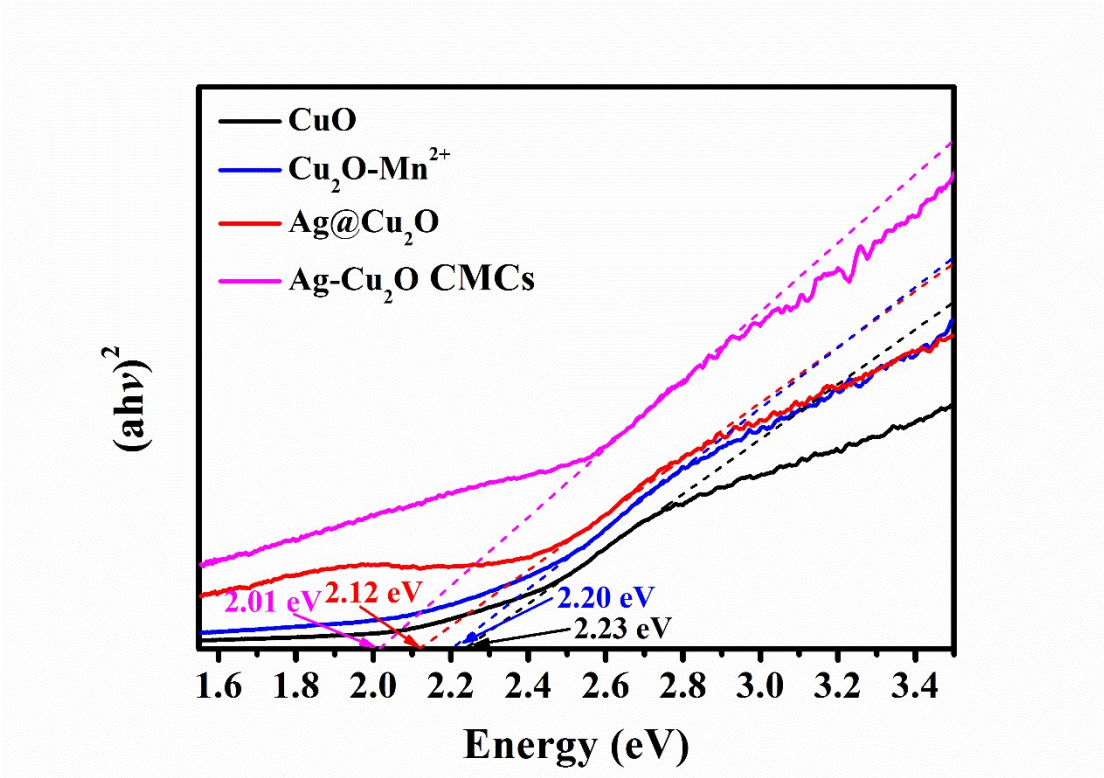

Figure S10. The plot of $(\alpha h\nu)^2$ versus photon energy based on UV-vis DRS spectra.

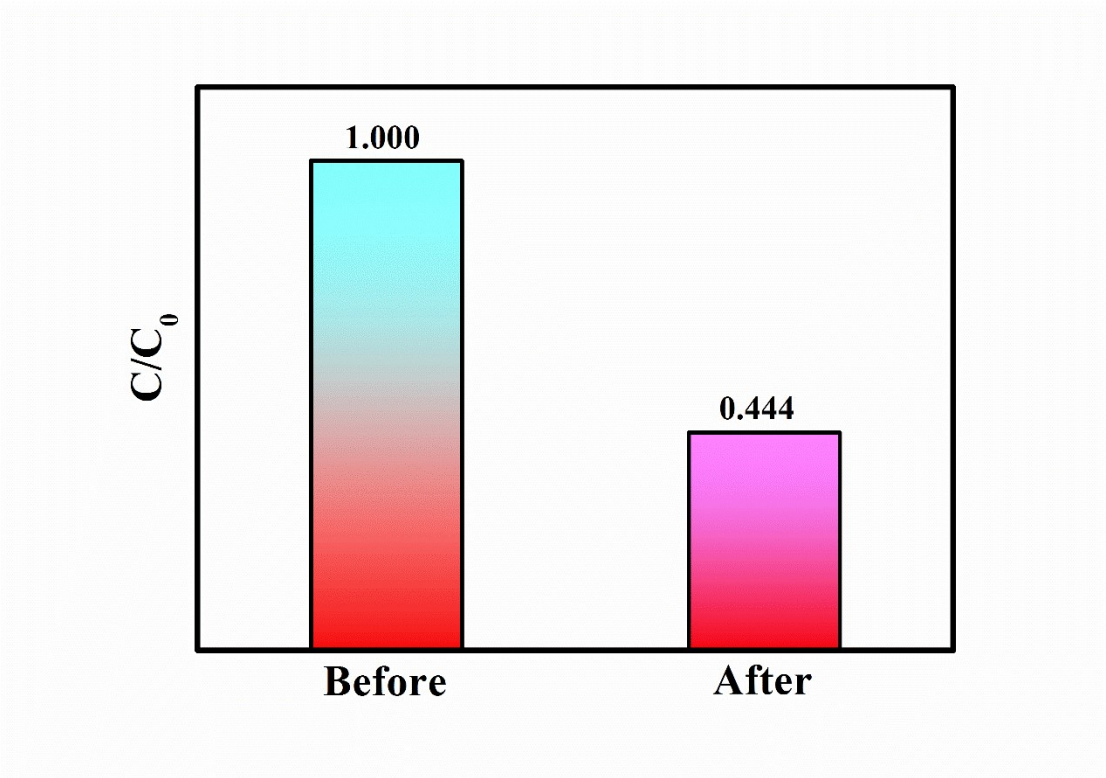

Figure S11. For Ag-Cu_2O CMCs sample, TOC content of TC solution before and after light irradiation for 120 min.

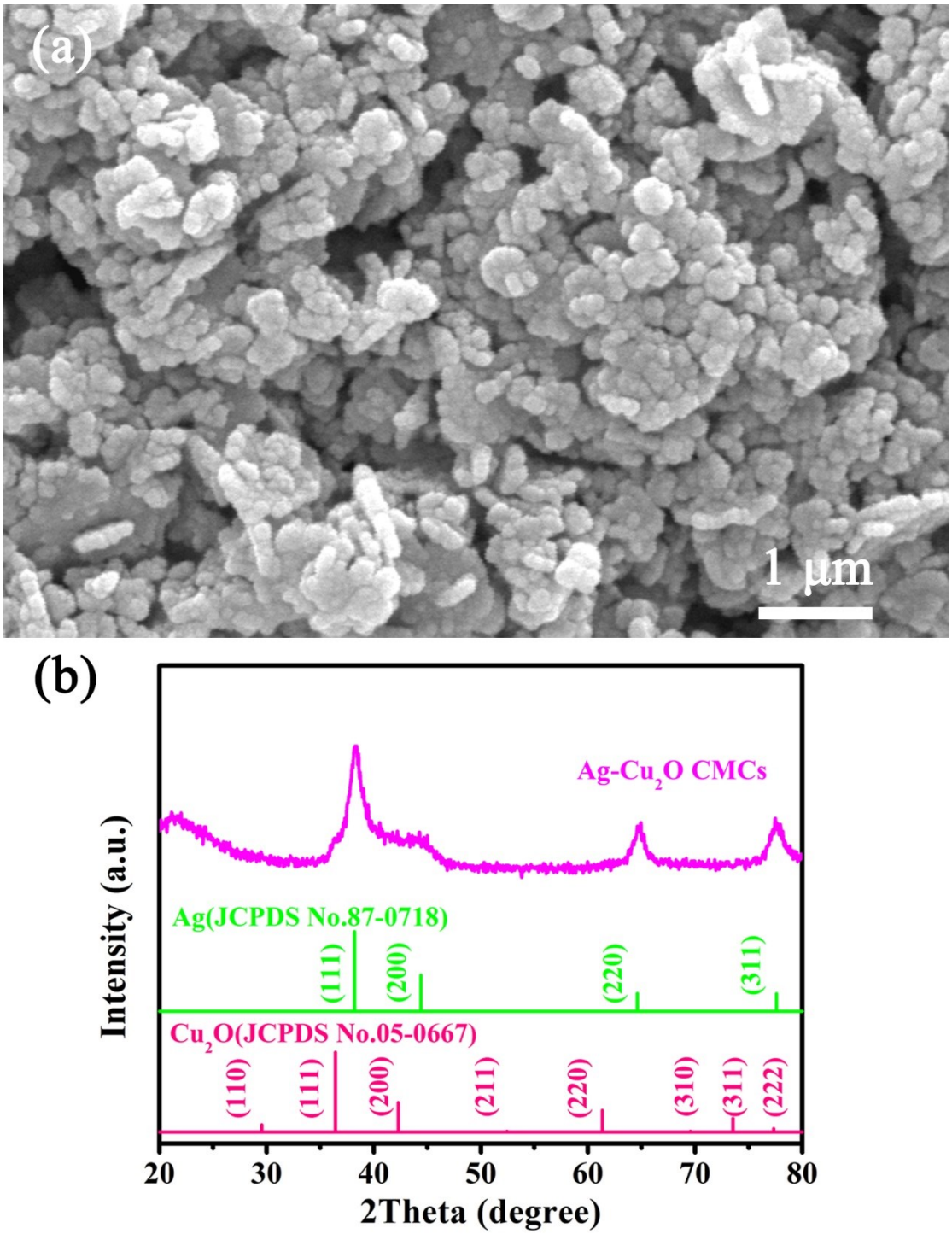

Figure S12. (a) SEM image and (b) XRD pattern of the Ag-Cu_2O CMCs sample after photodegradation of TC solution.

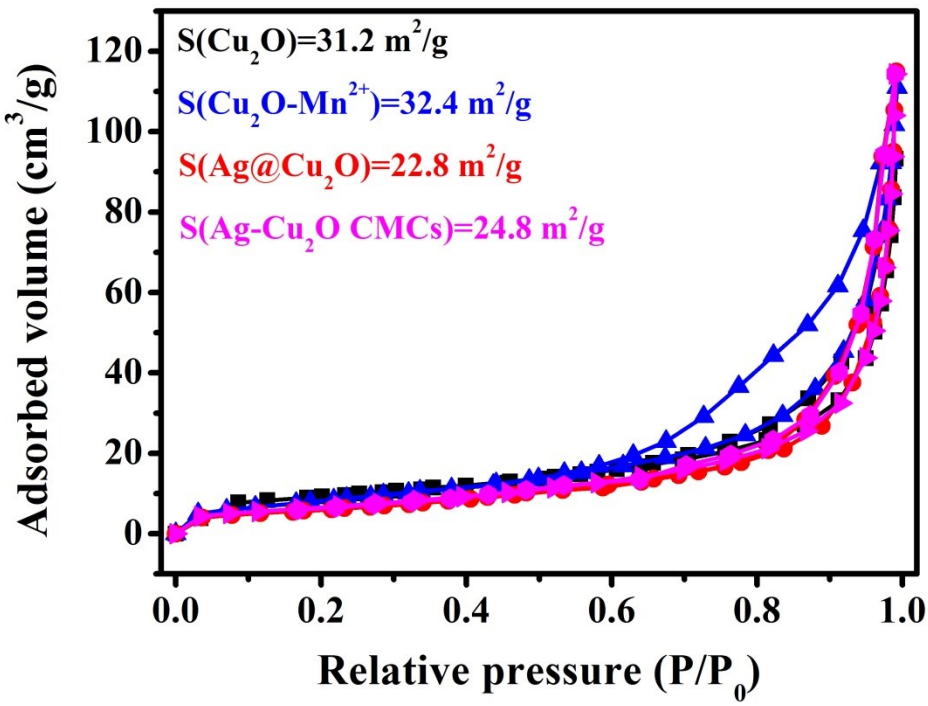

Figure S13. Nitrogen gas adsorption-desorption isotherms and BET surface areas of the Ag-Cu_2O CMCs, Ag@Cu_2O, Cu_2O-Mn^{2+} and Cu_2O samples.